Dispersive Fractalization in Fermi–Pasta–Ulam Lattices
I. The Linear Regime

Peter J. Olver
School of Mathematics
University of Minnesota
Minneapolis, MN 55455
olver@umn.edu
http://www.math.umn.edu/∼olver

Abstract. We investigate dispersive quantization and fractalization of the periodic linear Fermi–Pasta–Ulam system.

Our problem turned out to have been felicitously chosen. The results were entirely different qualitatively from what even Fermi, with his great knowledge of wave motions, had expected. ... To our surprise, the string started playing a game of musical chairs, only between several low notes, and perhaps even more amazingly, after what would have been several hundred ordinary up and down vibrations, it came back almost exactly to its original sinusoidal shape.

— Stanislaw Ulam, [**34**; pp. 226–7]

1. Introduction and Historical Perspective.

The Fermi–Pasta–Ulam (FPU) problem, [**15**], modeling the dynamics of mass–spring chains with nonlinear restoring forces, is celebrated as one of the very first electronic computer experiments, and certainly the first that produced novel behavior. The surprise was that the FPU dynamics was, at least on moderately long time intervals, not ergodic as expected, but rather exhibited recurrence in which energy from the low frequency modes would initially spread into the higher modes but, after a certain time period, mostly return to its initial configuration, as in the above quote from Ulam's autobiography. In an attempt to understand this phenomenon, Zabusky and Kruskal, [**40**], derived a continuum model

February 27, 2019

that, in its unidirectional manifestation, turned out to be the Korteweg–deVries (KdV) equation, originally derived by Boussinesq, [**5**], in his pioneering studies of surface water waves. Zabusky and Kruskal's numerical integration of the periodic initial-boundary value problem for the Korteweg–deVries equation, starting with a smooth initial profile, led to their discovery of the soliton[†] and the consequent creation of an entirely new branch of mathematics — integrable nonlinear partial differential equations, whose remarkable repercussions continue to this day, [**11**].

In a completely unrelated but also surprising development, in the early 1990's, Michael Berry and collaborators, [**1**, **2**, **3**], discovered the Talbot effect, which they named after a 1835 optical experiment of the Victorian scientist, inventor, and photography pioneer William Henry Fox Talbot, [**32**]. The effect arises in quantum mechanics through the behavior of rough solutions to the free space linear Schrödinger equation on a circular domain, i.e., subject to periodic boundary conditions. The evolution of a piecewise smooth but discontinuous initial profile, e.g., a step function, produces a fractal profile at irrational times (relative to the circumference of the circle) but "quantizes" into piecewise smooth but discontinuous profiles at rational times. Moreover, the fundamental solution, induced by an initial delta function, exhibits "revivals" at rational times, localizing into a finite linear combination of delta functions. This has the astonishing consequence that, at rational times, the solution to *any* periodic initial value problem is a finite linear combination of translates of the initial data and hence its value at any point on the circle depends only upon finitely many of the initial values! The effect underlies the experimentally observed phenomenon of quantum revival, [**3**, **37**, **35**], in which an electron, say, that is initially concentrated at a single location of its orbital shell is, at rational times, re-concentrated at a finite number of orbital locations.

The subsequent rediscovery of this remarkable phenomenon by the author, in the context of the periodic linearized Korteweg–deVries equation, [**20**, **21**], showed that fractalization and, at times, quantization phenomena appear in a wide range of linear dispersive (integro-)differential equations, including models arising in fluid mechanics, plasma dynamics, elasticity, DNA dynamics, and elsewhere. Such linear systems exhibit a fascinating range of as yet poorly understood dynamical behaviors, whose qualitative features are tied to the large wave number asymptotics of the underlying dispersion relation. These studies were then extended, through careful numerical simulations, [**8**], to show that fractalization and quantization also appear in a variety of nonlinear dispersive equations, including integrable models, such as the nonlinear Schrödinger, Korteweg–deVries, and modified Korteweg–deVries equations, as well as their non-integrable generalizations with higher degree nonlinearities. (It is interesting to speculate as to how the history of the subject might have changed were Zabusky and Kruskal to have started their investigations with discontinuous initial data!) Some of these numerical observations were subsequently rigorously confirmed in papers of Erdoğan and collaborators, [**9**, **12**, **13**, **14**]; see also earlier analytical work of Oskolkov, [**24**], and Rodnianski, [**26**].

Given that the Korteweg–deVries equation and its generalizations arise as continuum

[†] Although, the "solitons" they observed were in fact finite gap solutions composed of cnoidal waves, true solitons only arising when the equation is posed on the entire real line.

models for FPU chains, the question naturally arises as to whether dispersive fractalization and quantization effects appear in the discrete FPU system. Resolving this question is the aim of this paper and its sequel(s). In this first installment, we focus our attention on the much simpler linear system, which can be analytically integrated. We find that, on an appropriately long time scale, the solutions to the periodic linear FPU chain subject to a step function initial displacement do exhibit a suitably interpreted discrete version of fractalization and (approximate) quantization. On the other hand, we were unable to detect any trace of revival in the discrete system, which remains not entirely understood. The second paper in the series will extend our analysis to the fully nonlinear systems.

2. The Fermi–Pasta–Ulam Chain and its Continuum Models.

The Fermi–Pasta–Ulam (FPU) lattice consists of a one-dimensional chain of masses that are connected by springs with nonlinear restoring forces, [**15**, **25**]. We will only consider the case when both the masses and chains are identical, noting that more general systems have also been investigated in the literature, [**6**, **16**]. The dynamics of the mass-spring chain follows immediately from Newton's Laws, and takes the form of a system of second order ordinary differential equations for the mass displacements $u_n(t)$ for $n \in \mathbb{Z}$ at time t:

$$\begin{aligned} \mu^{-2}\, \frac{d^2 u_n}{dt^2} &= F(u_{n+1} - u_n) - F(u_n - u_{n-1}) \\ &= u_{n+1} - 2\,u_n + u_{n-1} + N(u_{n+1} - u_n) - N(u_n - u_{n-1}), \end{aligned} \tag{2.1}$$

where μ is the resonant frequency of the linear spring. The forcing function has the form

$$F(y) = y + N(y) = V'(y), \qquad \text{with potential} \qquad V(y) = \tfrac{1}{2}\, y^2 + W(y), \tag{2.2}$$

where y indicates the elongation of an individual spring. The nonlinear intermass forcing term is prescribed by $N(y) = W'(y)$. As in [**38**, **40**], we will focus attention on the quadratic case when

$$N(y) = \alpha\, y^2, \tag{2.3}$$

although higher degree polynomials in y, particularly cubic, are also of great interest. Another important system is the integrable Toda lattice, [**33**], where

$$V(y) = \alpha\, e^{\beta\, y}. \tag{2.4}$$

Other important examples include the Calogero–Moser integrable system and its trigonometric, hyperbolic, and elliptic generalizations, [**7**, **19**, **31**], where

$$V(y) = \frac{\alpha}{y^2} \quad \text{or} \quad V(y) = \frac{\alpha}{\sin^2 y} \quad \text{or} \quad V(y) = \frac{\alpha}{\sinh^2 y} \quad \text{or} \quad V(y) = \mathcal{P}(y), \tag{2.5}$$

with $\mathcal{P}$ the Weierstrass elliptic function, as well as the Lennard–Jones potential, [**18**],

$$V(y) = \frac{\alpha}{y^{12}} - \frac{\beta}{y^6}, \tag{2.6}$$

which is used to model interactions between atoms and molecules.

In this note, we will concentrate on the periodic problem, viewing the system as a circular chain consisting of m masses, which are labelled so that $u_k(t) = u_l(t)$ whenever $k \equiv l \bmod m$. Another important case is an infinite chain, with the displacements at large distances subject to suitable decay conditions. Since the continuum models have smooth evolutionary behavior on the line — dispersive quantization being intimately tied to the periodic boundary conditions — we do not anticipate any unexpected effects in an infinite FPU chain and so do not pursue it here. The *Dirichlet problem* in which the first and last masses are pinned down, so that $u_0(t) = u_m(t) = 0$, with $n = 0, \dots, m$, is also of interest, [**38**], but its analysis will be deferred.

Following [**40**, **38**, **27**, **28**], we endeavor to better understand the discrete FPU dynamics by passing to a continuum model. To this end, we assume the masses lie on a circle of fixed radius, say the unit circle of circumference 2π. As the number of masses $m \to \infty$, the equilibrium intermass spacing $h = 2\pi/m \to 0$. To maintain consistency, the time must be correspondingly rescaled, $t \mapsto h\,t$, and so we consider the system

$$\frac{d^2 u_n}{dt^2} = \frac{c^2}{h^2}\big[\, F(u_{n+1} - u_n) - F(u_n - u_{n-1}) \,\big], \tag{2.7}$$

where $c = \mu\, h$ will be the wave speed of the limiting scalar wave equation.

We can view the individual displacements as the sample values of an interpolating function $u(t, x)$ that is 2π periodic in x, so that

$$u_n(t) = u(t, x_n), \qquad \text{where} \qquad x_n = n\,h = \frac{2\pi\, n}{m}$$

are the nodes or reference positions of the masses. To produce a continuum model, we apply Taylor's theorem to expand

$$u_{n\pm1}(t) = u(t, x_n \pm h) = u \pm h\, u_x + \tfrac{1}{2}\, h^2 u_{xx} \pm \tfrac{1}{6}\, h^3 u_{xxx} + \ \cdots\ ,$$

where the right hand side is evaluated at (t, x_n). Substituting into (2.1) and replacing $x_n \mapsto x$, we arrive at the dispersive partial differential equation

$$u_{tt} = c^2\big(K[u] + M[u]\big), \tag{2.8}$$

with linear component

$$K[u] = u_{xx} + \tfrac{1}{12} h^2 u_{xxxx} + \mathrm{O}(h^4), \tag{2.9}$$

while $M[u]$ is obtained by similarly expanding the nonlinear terms. For example, in the quadratic case[†] (2.3),

$$M[u] = 2\,\alpha\, h\, u_x u_{xx} + \tfrac{1}{6}\,\alpha\, h^3\big(u_x u_{xxxx} + 2\, u_{xx} u_{xxx}\big) + \mathrm{O}(h^5). \tag{2.10}$$

Thus, assuming the linear wave speed c and nonlinear scale parameter α are both $\mathrm{O}(1)$, we obtain, to second order in h, the bidirectional continuum model

$$u_{tt} = c^2\big(u_{xx} + 2\,\alpha\, h\, u_x u_{xx} + \tfrac{1}{12} h^2 u_{xxxx}\big), \tag{2.11}$$

[†] For unexplained reasons, Zabusky, [**38**], is missing the term involving $u_x u_{xxxx}$.

a potential form of the integrable (nonlinear) *Boussinesq equation*, [**11**],

$$v_{tt} = c^2\big(v_{xx} + \alpha\, h\,(v^2)_{xx} + \tfrac{1}{12} h^2 v_{xxxx}\big), \tag{2.12}$$

which can be obtained by differentiating (2.11) with respect to x and replacing $u_x \mapsto v$. Note that, to leading order, the continuum model (2.11) coincides with the standard linear wave equation $u_{tt} = c^2 u_{xx}$ with wave speed $c > 0$. The *Korteweg–deVries equation* is obtained through a standard "unidirectional factorization" of the preceding bidirectional system, [**36**], i.e., assuming the waves are only propagating in one direction, say in the direction of increasing x, producing

$$u_t + c\,\big(u_x + \alpha\, h\, u\, u_x + \tfrac{1}{24} h^2 u_{xxx}\big) = 0. \tag{2.13}$$

Remark: For the cubically forced FPU system, the unidirectional model is the integrable modified Korteweg-deVries equation, [**28**, **38**], in which the nonlinear term is a multiple of $u^2 u_x$. Higher degree forcing polynomials produce generalized Korteweg–deVries equations with higher degree nonlinearities, which are no longer integrable, and, in fact, can produce blow up of solutions, [**4**].

Let us from here on ignore the nonlinear contributions and concentrate on the linear FPU system and its continuum models. (Extending our analysis to nonlinear FPU chains will be the subject of subsequent papers in this series.) The rescaled linear FPU system (2.7) becomes what is known as the *discrete wave equation*, [**25**]:

$$\frac{d^2 u_n}{dt^2} = \frac{c^2}{h^2}\big(u_{n+1} - 2\,u_n + u_{n-1}\big), \tag{2.14}$$

which, to the same order in h, has bidirectional continuum model

$$u_{tt} = c^2\big(u_{xx} + \tfrac{1}{12}\, h^2 u_{xxxx}\big), \tag{2.15}$$

known as the linearized "bad Boussinesq equation", [**27**], owing to the fact that it is an ill-posed partial differential equation. Indeed, its dispersion relation is found by the usual method, [**36**], of substituting the exponential ansatz

$$u(t,x) = e^{\,\mathrm{i}\,(k\,x - \omega\, t)}, \tag{2.16}$$

producing the algebraic equation

$$\omega^2 = p_4(k) = c^2 k^2\big(1 - \tfrac{1}{12}\, h^2 k^2\big) \tag{2.17}$$

relating the temporal frequency ω to the wave number (spatial frequency) k. Because $p_4(k) < 0$ for $k \gg 0$, the bad Boussinesq model (2.15) is *not* purely dispersive since the high wave number modes induce complex conjugate purely imaginary values of ω and hence exponentially growing modes, [**10**], that induce the ill-posedness of the initial value problem. Interestingly, the linearized unidirectional Korteweg–deVries model

$$u_t + c\,\big(u_x + \tfrac{1}{24} h^2 u_{xxx}\big) = 0 \tag{2.18}$$

does not suffer from this instability, since its dispersion relation is

$$\omega = c\,k\big(1 - \tfrac{1}{24}\, h^2 k^2\big), \tag{2.19}$$

which coincides with the Taylor expansion, at $k = 0$, of one of the two branches of the bidirectional dispersion relation (2.17). The corresponding linearized *bidirectional Korteweg–deVries equation*

$$u_{tt} = \big(c\partial_x + \tfrac{1}{24}\, c h^2 \partial_x^3\big)^2 u = c^2\big(u_{xx} + \tfrac{1}{12}\, h^2 u_{xxxx} + \tfrac{1}{576}\, h^4 u_{xxxxxx}\big), \tag{2.20}$$

has solutions that are an exact linear combination of right- and left-moving linear KdV solutions. Positivity of the right hand side of the corresponding dispersion relation

$$\omega^2 = c^2k^2\big(1 - \tfrac{1}{24}\, h^2k^2\big)^2 = c^2k^2\big(1 - \tfrac{1}{12}\, h^2k^2 + \tfrac{1}{576}\, h^4k^4\big) \tag{2.21}$$

implies well-posedness of this sixth order model.

Remark: It remains somewhat mysterious to the author how an ill-posed bidirectional wave model can have right- and left-moving unidirectional constituents that are both well-posed. This is clearly a consequence of the use of low wave number Taylor expansions of the dispersion relation near $k = 0$ in the approximation procedure, but I would argue that this seeming paradox warrants further study.

Another means of regularizing the linear, and hence the nonlinear, continuum model is to retain the order h^4 terms in the preceding Taylor expansion. This produces the sixth order linear partial differential equation

$$u_{tt} = c^2\big(u_{xx} + \tfrac{1}{12}\, h^2 u_{xxxx} + \tfrac{1}{360}\, h^4 u_{xxxxxx}\big), \tag{2.22}$$

with dispersion relation

$$\omega^2 = p_6(k) = c^2k^2\big(1 - \tfrac{1}{12}\, h^2k^2 + \tfrac{1}{360}\, h^4k^4\big). \tag{2.23}$$

Since $p_6(k) > 0$ for all k, the regularized model (2.22) is purely dispersive, and hence well-posed, in that all Fourier modes maintain their form under translation.

An alternative regularization procedure that avoids increasing the order of the differential equation is to replace two of the x derivatives in the fourth order term in the bad Boussinesq equation (2.15) by t derivatives, using the fact that, to leading order, $u_{xx} = c^{-2}u_{tt} + \mathrm{O}(h^2)$, thereby producing the continuum model

$$u_{tt} = c^2 u_{xx} + \tfrac{1}{12}\, h^2 u_{xxtt}, \tag{2.24}$$

known as the *linear Boussinesq equation*, [**36**; pp. 9, 462], which arises as the linearization of Boussinesq's bidirectional model for shallow water waves, which was also proposed as a model for DNA dynamics, [**29**]. In this case, the dispersion relation is

$$\omega^2 = q(k) = \frac{c^2k^2}{1 + \frac{1}{12}\, h^2k^2} \approx c^2k^2\big(1 - \tfrac{1}{12}\, h^2k^2 + \tfrac{1}{144}\, h^4k^4 + \,\cdots\big) > 0, \tag{2.25}$$

and hence the equation is purely dispersive and well-posed.

Let us next derive the analogous "dispersion relation" for the discrete FPU system (discrete wave equation) (2.14); see also [**39**]. Substituting the usual exponential ansatz

(2.16), evaluated at the node $x = x_n = n\,h$, into (2.14) produces

$$\begin{aligned} -\omega^2 e^{\,\mathrm{i}\,(k\,x_n - \omega\,t)} &= \frac{c^2}{h^2}\big(e^{\,\mathrm{i}\,(k\,x_n + k\,h - \omega\,t)} - 2\,e^{\,\mathrm{i}\,(k\,x_n - \omega\,t)} + e^{\,\mathrm{i}\,(k\,x_n - k\,h - \omega\,t)}\big) \\ &= -\,\frac{2\,c^2}{h^2}(1 - \cos k\,h)\,e^{\,\mathrm{i}\,(k\,x_n - \omega\,t)}. \end{aligned} \tag{2.26}$$

We thus deduce the discrete FPU dispersion relation

$$\omega^2 = \frac{2\,c^2}{h^2}(1 - \cos k\,h) = \frac{4\,c^2}{h^2}\sin^2 \tfrac{1}{2}\,k\,h = \frac{c^2 m^2}{\pi^2}\sin^2 \frac{k\,\pi}{m} \tag{2.27}$$

that determines the temporal frequencies ω in terms of the wave numbers k. Since $\omega(k)$ is real for all $k = 0, \dots, n$, the FPU system can be regarded as dispersive, in that the different Fourier modes propagate unchanged at different wave speeds, implying "well-posedness" or, more accurately since we are dealing with a system of ordinary differential equations, stability of the zero equilibrium solution. Moreover, observe that the continuum model dispersion relations (2.17), (2.23), (2.21), and (2.25) all have the same order h^4 Taylor expansion at $k = 0$ as (2.27), and hence approximate it well at low or even moderately large wave numbers. However, they exhibit different high wave number asymptotics, which, as noted in [**8**], is the key property that governs the dispersive fractalization of rough solutions.

3. The Riemann Problem.

As in [**8**, **20**], we are particularly interested in the *Riemann problem*, of fundamental importance in the study of hyperbolic wave equations and shock waves, [**30**]. Here, the initial displacement is a (periodically extended) step function:

$$u(0,x) = \begin{cases} 1, & 0 < x < \pi, \\ 0, & -\pi < x < 0, \\ \frac{1}{2}, & x = -\pi,\ 0,\ \pi, \end{cases} \tag{3.1}$$

whose values at integer multiples of π are specified in accordance with the convergence properties of its Fourier series

$$u(0,x) = \frac{1}{2} + \frac{2}{\pi}\sum_{j=0}^{\infty} \frac{\sin(2\,j+1)\,x}{2\,j+1}\,. \tag{3.2}$$

We will also, for simplicity, impose zero initial velocity, concentrating on the pure displacement problem:

$$u_t(0,x) = 0, \tag{3.3}$$

leaving the analysis of the effects of a nonzero initial velocity to a subsequent study. Given a well-posed linear bidirectional continuum model equation, such as (2.20), (2.22), or (2.24), with associated dispersion relation $\omega(k)$, the Fourier series for the solution to the

corresponding periodic initial value problem (3.1, 3) takes the form of a linear combination of standing wave solutions:

$$u(t,x) = \frac{1}{2} + \frac{2}{\pi} \sum_{j=0}^{\infty} \frac{\cos \omega(2j+1)\,t \;\; \sin{(2j+1)\,x}}{2j+1}\,. \tag{3.4}$$

By an elementary trigonometric identity, we can split the standing wave summands in (3.4) into right- and left-moving unidirectionally propagating waves:

$$u(t,x) = \frac{u_{\scriptscriptstyle R}(t,x) + u_{\scriptscriptstyle L}(t,x)}{2}, \tag{3.5}$$

where the factor of $\frac{1}{2}$ is introduced for comparative purposes, whereby all three solutions have the same initial displacement:

$$u(0,x) = u_{\scriptscriptstyle R}(0,x) = u_{\scriptscriptstyle L}(0,x).$$

The right-moving constituent is

$$u_{\scriptscriptstyle R}(t,x) = \frac{1}{2} + \frac{2}{\pi} \sum_{j=0}^{\infty} \frac{\sin\big[\,(2j+1)\,x - \omega(2j+1)\,t\,\big]}{2j+1}\,, \tag{3.6}$$

and its left-moving counterpart is obtained by replacing t by $-t$.

The corresponding step function initial data for the discrete FPU problem is obtained by sampling (3.1) at the nodes $x = x_{\scriptscriptstyle n} = n\,h = 2\,\pi\,n/m$, whence

$$u_{\scriptscriptstyle n}(0) = \begin{cases} 1, & 0 < n < m, \\ 0, & -m < n < 0, \\ \frac{1}{2}, & n = -m,\ 0,\ m. \end{cases} \tag{3.7}$$

In other words, we displace each mass lying on the "right semicircle" by 1 unit, while those on the left remain at their equilibrium position, except the two masses lying at the interface that are displaced by only half a unit. As in (3.3), the masses are assumed to be at rest initially:

$$\dot{u}_{\scriptscriptstyle n}(0) = 0. \tag{3.8}$$

We use the Discrete Fourier Transform to write the solution as a Fourier sum

$$u(t,x) \sim \sum_{k=1-m}^{m} c_{\scriptscriptstyle k}(t) e^{\,\mathrm{i}\,k\,x}, \tag{3.9}$$

over the fundamental periodic modes, [**22**; Section 5.6], where $\sim$ means that the left and right hand sides agree at the nodes, i.e., when $x = x_{\scriptscriptstyle n}$. The Discrete Fourier Transform applied to the sampled step function produces the interpolating discrete Fourier sum†

$$u(0,x) \;\sim\; \frac{1}{2} + \frac{1}{m} \sum_{j=0}^{[m/2]} \cot \frac{(2j+1)\,\pi}{2m} \;\; \sin(2j+1)\,x. \tag{3.10}$$

† The bracket on $[m/2]$ denotes the integer part.

In view of the dispersion relation (2.27), the resulting solution to the linearized FPU chain is

$$u(t,x) \sim \frac{1}{2} + \frac{1}{m} \sum_{j=0}^{[m/2]} \cot \frac{(2j+1)\pi}{2m} \cos\left(\frac{cmt}{\pi} \sin \frac{(2j+1)\pi}{m} \right) \sin(2j+1)x, \qquad (3.11)$$

meaning that the displacement of the n^{th} mass is given by sampling the right hand side at the nodes:

$$u_n(t) = u(t, x_n), \qquad x_n = nh = \frac{2\pi n}{m}. \qquad (3.12)$$

Again, the solution (3.11) is a linear combination of standing waves, and can be decomposed into left and right moving constituents, as in (3.5). The right-moving constituent has the explicit form

$$u_R(t,x) \sim \frac{1}{2} + \frac{1}{m} \sum_{j=0}^{[m/2]} \cot \frac{(2j+1)\pi}{2m} \sin\left((2j+1)x - \frac{cmt}{\pi} \sin \frac{(2j+1)\pi}{m} \right). \qquad (3.13)$$

As above, its left-moving counterpart is obtained by replacing t by $-t$.

Remark: Note that if we omit the constant term, the bidirectional solutions constructed in (3.4, 11) also satisfy Dirichlet boundary conditions, with a half-size signum function as initial condition: $u(t,x) = \frac{1}{2} \operatorname{sgn} x$, $-\pi < x < \pi$. Thus, all our subsequent remarks on their behavior also apply to this Dirichlet initial-boundary value problem. On the other hand, their unidirectional constituents do not individually satisfy Dirichlet boundary conditions.

As shown in [**20**, **24**], the canonical linearized Korteweg–deVries equation

$$u_\tau + u_{\xi\xi\xi} = 0 \qquad (3.14)$$

with step function initial data and periodic boundary conditions on $-\pi \le \xi \le \pi$ exhibits dispersive fractalization and quantization in the following sense. At *irrational times*, meaning $\tau/\pi \notin \mathbb{Q}$, the solution profile $u(\tau, \xi)$ is a continuous but non-differentiable fractal. On the other hand, at rational times, $\tau/\pi \in \mathbb{Q}$, the solution is discontinuous, but piecewise constant! Indeed, if $\tau = 2\pi p/q$ where $p, q \in \mathbb{Z}$ have no common factors, then the solution is constant on the intervals $2\pi j/q < \xi < 2\pi(j+1)/q$ for $j \in \mathbb{Z}$. Thus, the larger the denominator q, the shorter the intervals of constancy. (It is possible that the solution achieves the same constant value on one or more adjacent intervals, and so an interval of constancy may be larger. See [**23**] for a number-theoretic investigation into when this occurs.) A rigorous proof of the fractal nature of the solution at irrational times, including the estimate that its fractal dimension d is bounded by $\frac{3}{2} \le d \le \frac{7}{4}$, can be found in [**12**].

The results of [**12**] imply that a linear evolutionary integro-differential equation with dispersion relation that is (in an appropriate sense) asymptotic to a power of k at large wave numbers, $\omega(k) \sim k^\alpha$ as $k \to \infty$, for $1 \ne \alpha > 0$, exhibits fractalization at almost all times, provided the initial data is of bounded variation, but not too smooth, meaning it does not lie in any Sobolev space H^β for $\beta > \frac{1}{2}$, i.e., its Fourier coefficients c_n decay

sufficiently slowly so that the series $\sum (1+n^2)^{\beta} |\, c_n \,|^2$ diverges. Moreover, if the asymptotic exponent α is integral, $2 \leq \alpha \in \mathbb{Z}$, numerical experiments, [**8**], indicate that the solution profiles quantize at other times, in the sense that they take a different form from the "generic" fractal profiles: piecewise smooth with either jumps or cusps, possibly with some much smaller fractal modulation superimposed. However, being so far based on numerical calculations, it is not yet known if the observed small scale fractals on the quantized profiles are genuine or just a manifestation of numerical error.

Warning: The fractal dimension of the graph of a function has the potential to be misleading. For example, the graph of the sinusoidal function $f(x) = \sin(1/x)$ has fractal dimension 2 even though it is perfectly smooth, even analytic, except at the singularity at $x = 0$. For this reason, the results in [**12**], while striking, are, at a deeper level, unsatisfying. It would be preferable to know, or at least have estimates on, the Hausdorff dimension of (sections of) such solution profiles; however this seems to be beyond current analytic capabilities.

Turning our attention to the linearized Korteweg–deVries model (2.18), the leading first order term cu_x represents linear transport moving at speed $-c$, and only affects the solution by an overall translation. We can map (2.18) to the preceding canonical form (3.14) by a Galilean shift to a moving coordinate frame, coupled with a rescaling of the time variable:

$$\xi = x - ct, \qquad \tau = \tfrac{1}{24}\, c h^2 t. \tag{3.15}$$

Due to the temporal scaling, the dispersive quantization pattern occurring in the solution to the canonical KdV equation (3.14) at a rational time $\tau = 2\pi p/q$ will now appear (suitably translated) at a much later time, namely $t = 48\pi p/(ch^2 q)$. Since the normalized model (3.14) exhibits quantization at *every* rational time, the same is true (modulo the scaling factor used to distinguish rational from irrational) of the FPU model version (2.18). However, in the latter model, at a rational time $t = \mathrm{O}(1)$, the denominator q will be very large, of order $\mathrm{O}(h^{-2})$, hence the intervals of constancy are extremely small, $\mathrm{O}(h^2)$, and thus undetectable at the physical level, with spatial scale $\Delta x = \mathrm{O}(h)$. At such scales, both physical and graphical, it will be practically impossible to distinguish such profiles from fractals.

Now let us compare the solution to the periodic Riemann initial value problem for the discrete linear Fermi–Pasta–Ulam system (2.14) with those of the three model equations: the bidirectional Korteweg–deVries model (2.20), the sixth order model (2.22), and the regularized Boussinesq model (2.24). For our numerical comparisons, we sum the same m modes in the discrete and continuous Fourier series and plot the resulting profile; in other words, we are performing exact (well, modulo floating point round off) computations on the truncated (discrete) Fourier series and not a numerical approximation. The initial data is a (periodically extended) step function. In the continuum models, one can work with either the continuous Fourier series representation of the initial data (3.2), or the corresponding discrete Fourier sum (3.10). However, in the given situations, we observe no appreciable differences between the solution profiles, and hence will use the discrete version in all figures representing solutions to the Riemann initial value problem. We fix the wave speed $c = 1$, and, for most of our numerical investigations, work with $m = 1024$

masses, so that $h = 2\pi/m \approx .006136$. Solutions for other numbers of masses have been calculated, and the overall conclusions are similar, although the fewer their number, the less pronounced some effects tend to be; see also below.

The first observation is that, on the time scale and resolution we are using, there is almost no noticeable difference between the sixth order and regularized Boussinesq models, and so we choose only to display the results for the latter. We will plot both the bidirectional solution $u(t, x)$, as given in (3.4), (3.11) and its unidirectional right-moving constituent (3.6), (3.13). We consider the effects at times that are selected from three regimes: what we will call *short times*, where $t = \mathrm{O}(1)$, *medium times*, where $t = \mathrm{O}(h^{-1})$, and *long times*, where $t = \mathrm{O}(h^{-2})$.

First, on short time scales, the solutions to all four models exhibit little appreciable difference. For example, consider the profiles at $t = \frac{1}{5}\pi$ graphed in Figure 1 — the top row being the full bidirectional solution and the bottom row its right-moving unidirectional constituent. The only noticeable difference is that, on closer inspection, the oscillatory (or perhaps fractal) perturbation that is superimposed upon the intervals of constancy is more concentrated near the discontinuities in the regularized Boussinesq and sixth order models, while in the FPU and KdV cases, the oscillations are slightly more spread out, particularly in their unidirectional constituents.

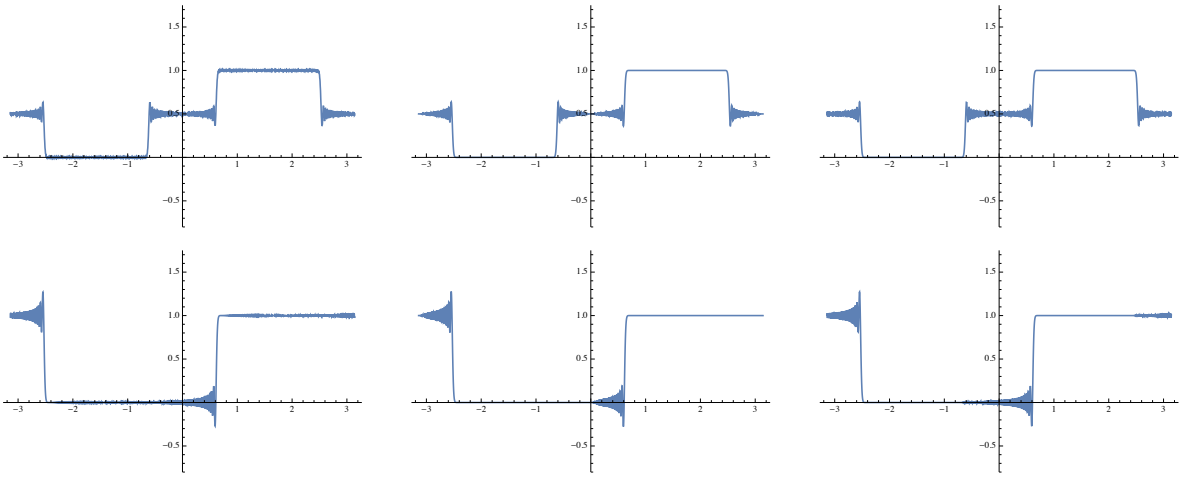

Figure 1. Bi- and uni-directional solution profiles at $t = \frac{1}{5}\pi$.

Since all profiles remain rather similar at short times, in Figure 2 we just graph the FPU solution profiles. What we observe is that, on the short time scale, the solution is an oscillatory perturbation of the traveling wave solution to the corresponding limiting bi- and uni-directional wave equations†

$$u_{tt} = u_{xx}, \qquad u_t + u_x = 0. \tag{3.16}$$

In particular, at $t = \frac{1}{2}\pi$, the right- and left-moving waves have cancelled each other out,

† Recall that we have set $c = 1$.

leaving only a constant solution profile for the traveling wave solution, with a superimposed fractal residue in the FPU system, as well as its continuum models, all three of which take on a comparable form.

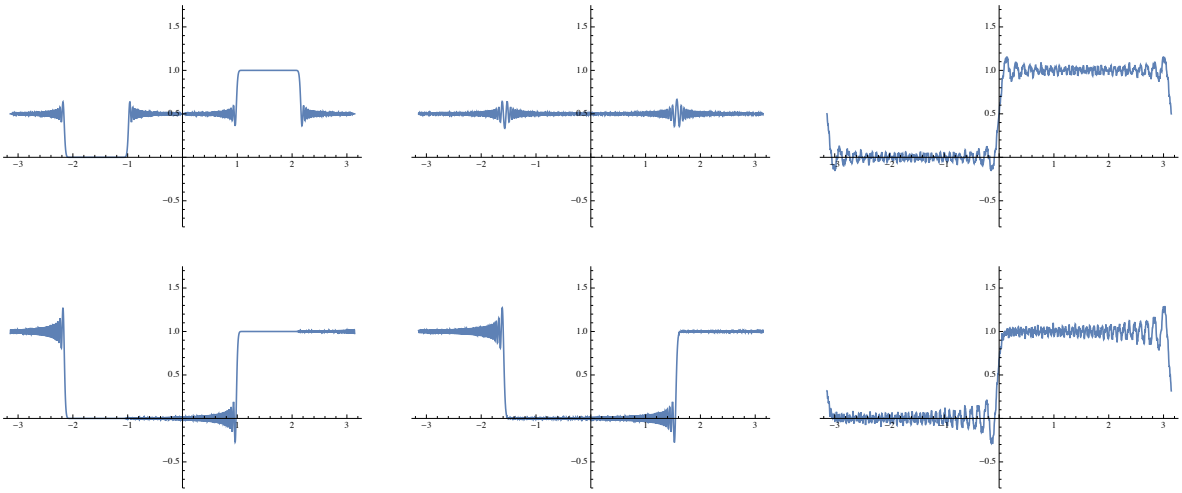

$t = 1$ $\qquad$ $t = \frac{1}{2}\pi$ $\qquad$ $t = 12\pi$

Figure 2. Bi- and uni-directional FPU solution profiles at short times.

At medium times, of order $O(h^{-1})$, the fractal nature of the oscillations superimposed upon the traveling wave solution profile has become more pronounced. Again, both the FPU system and its continuum models exhibit similar behavior; Figure 3 graphs the former at some representative medium times.

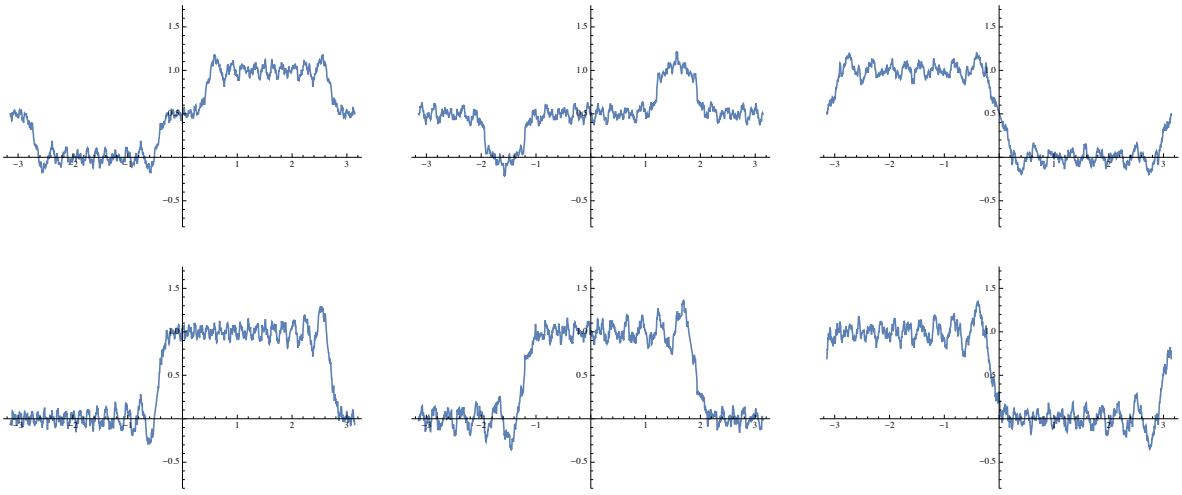

$t = 1/h$ $\qquad$ $t = 3/h$ $\qquad$ $t = \pi/h$

Figure 3. Bi- and uni-directional FPU solution profiles at medium times.

Once we transition to the long time scale, of order $O(h^{-2})$, significant differences arise in the observed behaviors. First consider the solution profiles at the irrational (meaning that $h^2\, t/\pi \notin \mathbb{Q}$) times $t = 1/h^2 \approx 26561$ and $t = 400000$, plotted in Figures 4 and 5; all three profiles are of a similar fractal form, albeit with differences in their small scale

features. The unidirectional constituents are more "pure" fractals, while the bidirectional solutions exhibit some semi-coherent regions, perhaps indicating some remnant of the intervals of constancy of a nearby rational profile.

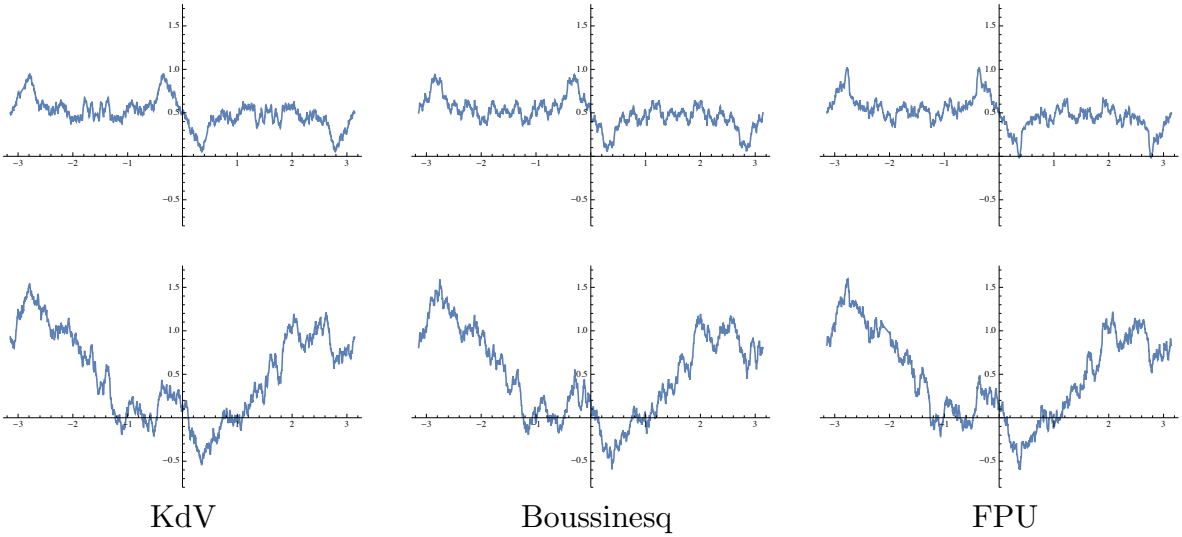

Figure 4. Bi- and uni-directional solution profiles at $t = 1/h^2 \approx 26{,}561$.

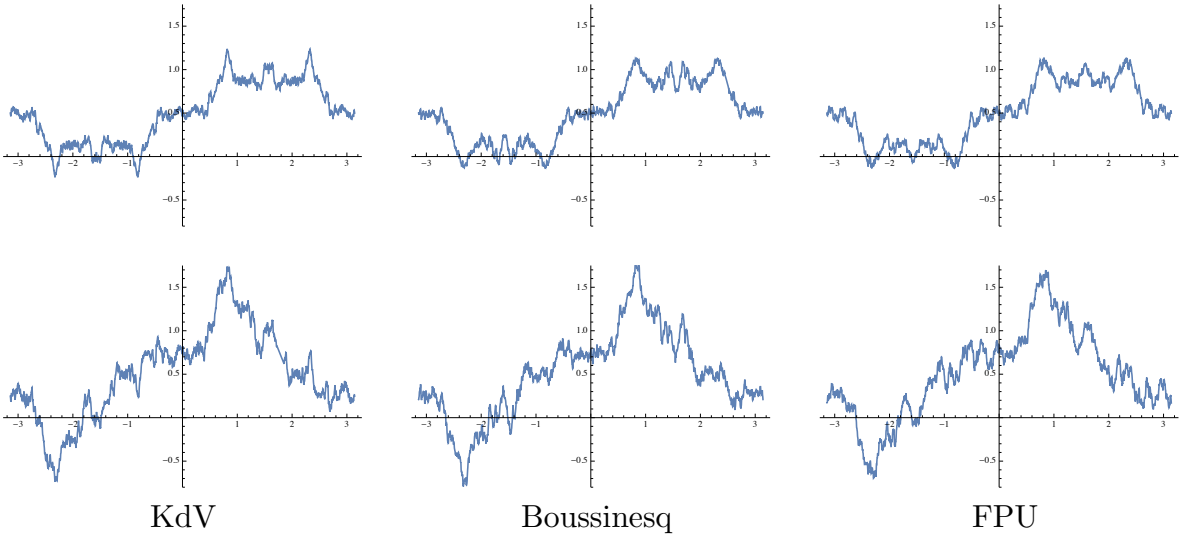

Figure 5. Bi- and uni-directional solution profiles at $t = 400{,}000$.

However, at long rational times, the solution profiles diverge dramatically, as illustrated in Figures 6 and 7 for two representative such times. The linearized KdV solution has quantized into a piecewise constant profile, whereas the FPU system and the Boussinesq models retain a common fractal form. On the other hand, the latter profiles exhibit an observable adherence to the underlying the piecewise constant KdV solution, albeit with a significant superimposed fractal modulation.

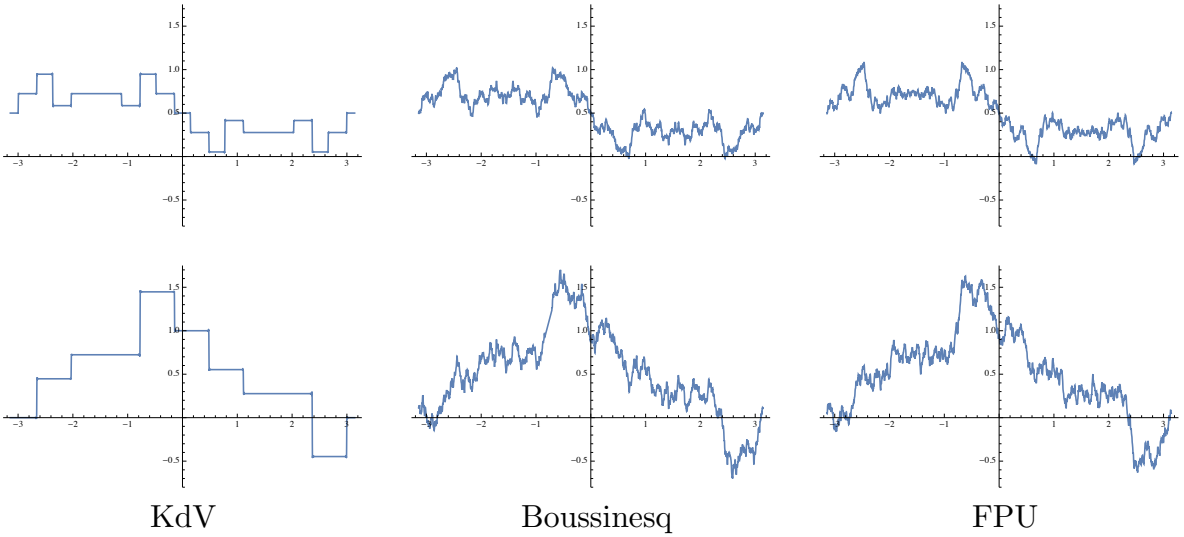

Figure 6. Bi- and uni-directional solution profiles at $t = 24\pi/(5h^2) \approx 400{,}527$.

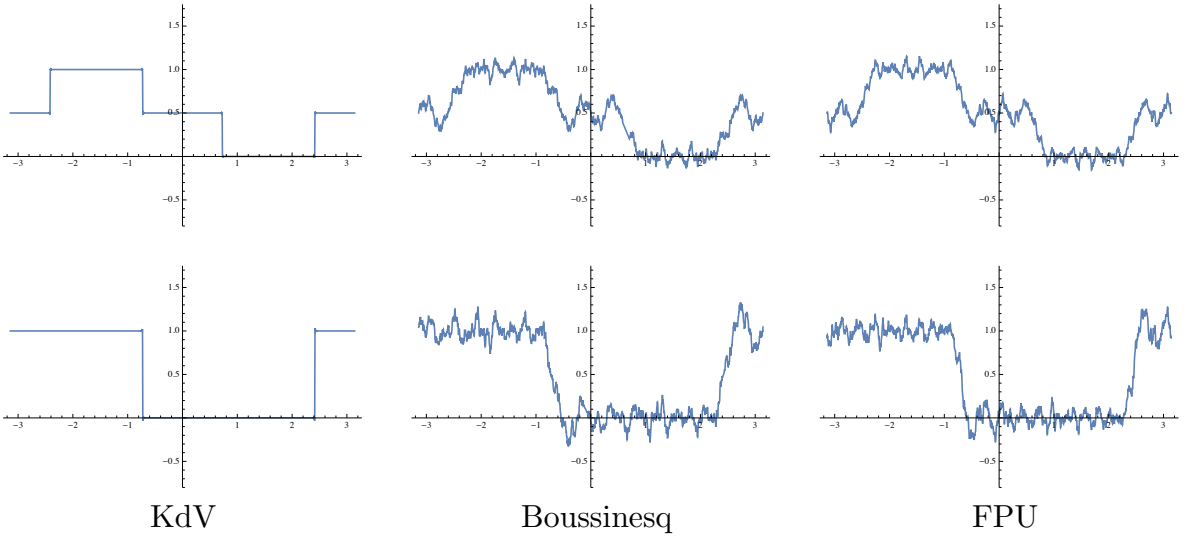

Figure 7. Bi- and uni-directional solution profiles at $t = 24\pi/h^2$.

Recall that the initial data is the discrete Fourier representation (3.10) of the step function. Interestingly, if we use the continuous version (3.2) instead, which only differs in its higher frequency modes, the graphs do not appreciably change, and so are not displayed. The only noticeable difference is that piecewise constant KdV profile exhibits a more pronounced Gibbs phenomenon at the discontinuities.

Now, one might argue that the reason for the difference between the quantized KdV profiles and the fractal FPU ones, lies in how the dispersion relation affects the high frequency modes. So one might try eliminating the higher frequency terms by truncating the Fourier sum in order to bring the solutions closer in spirit. It is surprising that one

must eliminate the vast majority of the high frequency modes before they begin to align at the rational quantized times, whereas at the irrational fractalized times the profiles are quite similar no matter how one truncates.

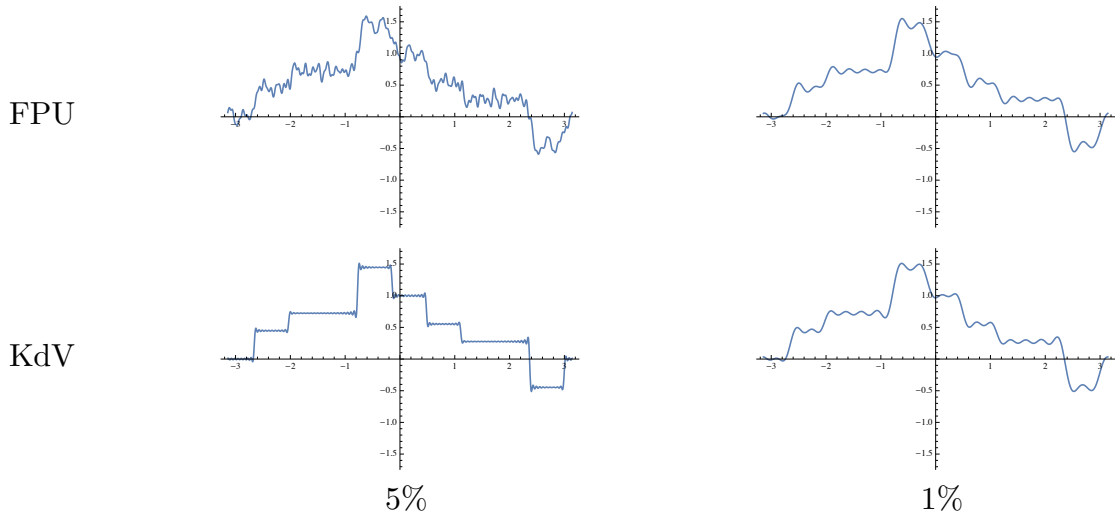

Figure 8. Truncated unidirectional solution profiles at $t = 24\pi/(5h^2) \approx 400{,}527$.

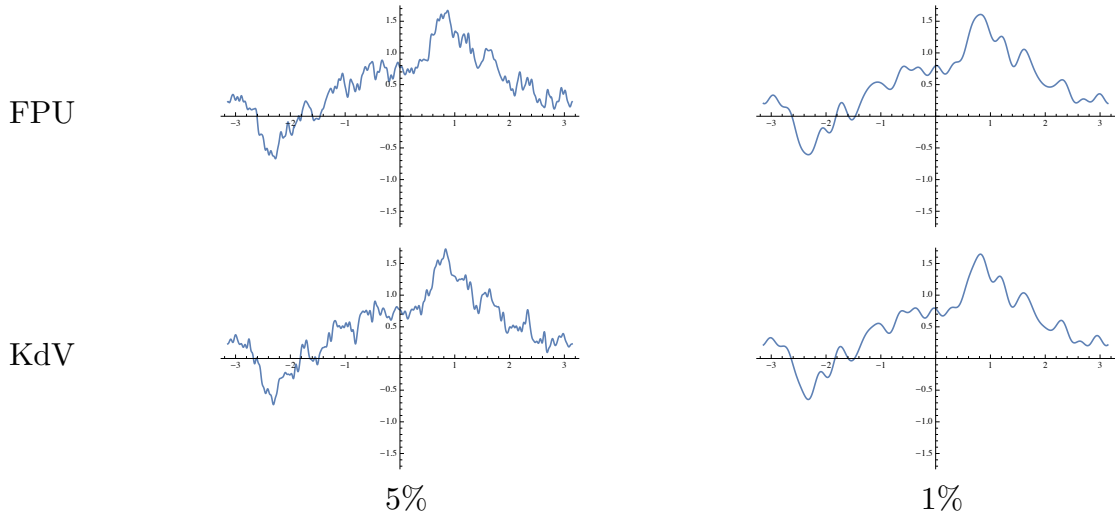

Figure 9. Truncated unidirectional solution profiles at $t = 400{,}000$.

Keeping in mind that we are working with $m = 1024$ total modes, the first plots in Figure 8 are at the same quantized time illustrated in Figure 6, and show the results of summing the first 5%, namely 51, and 1%, namely 10, of the terms in the full series. The top row shows the resulting truncated profiles for the unidirectional FPU solution (3.13), while the bottom row shows the corresponding truncated KdV profile (3.6). Somewhat surprisingly, even retaining 5% of the modes leads to significant differences, and only at the very coarse 1% scale do they look at all close. On the other hand, in Figure 9, which illustrates the same results at the irrational time that were shown in Figure 6, both

truncated profiles exhibit very similar features, while, as expected, the overall local fractal nature of the profile is curtailed as the number of terms decreases.

Of course, the FPU mass-spring chain is not a continuum, and so the values of the trigonometric solution (3.11) — or its unidirectional counterpart (3.13) — only have physical meaning at the mass nodes. For the above cases of $m = 1024$ masses, the differences are imperceptible. To better illustrate the differences, in Figure 10 we plot solution profiles for $m = 64$ masses, at selected times, comparing the discrete mass displacement profiles, the corresponding continuum FPU bidirectional solution (3.11), and the continuum bidirectional solution (3.4) with KdV dispersion (2.19). Observe that the effects are quite similar to what was presented above, but less pronounced owing to the relatively small number of masses.

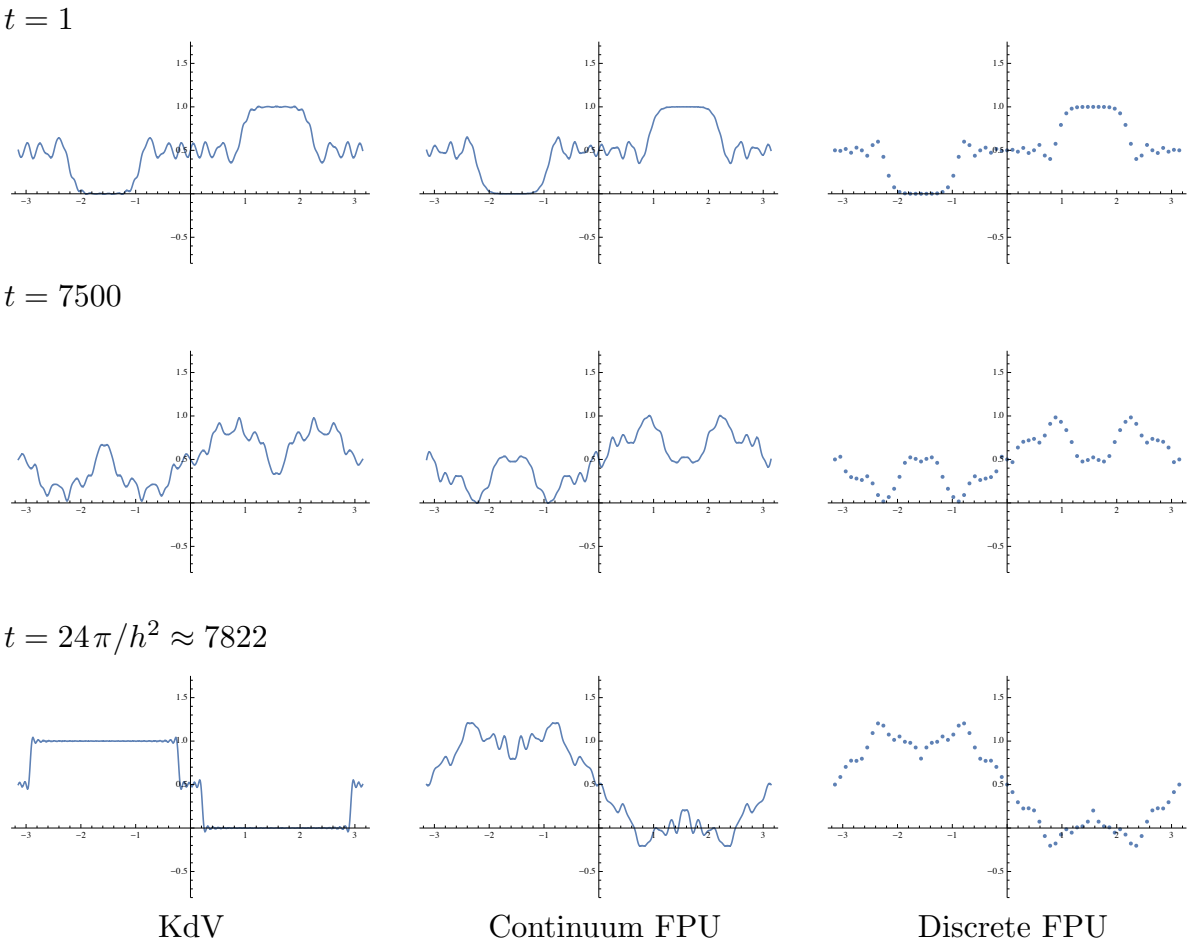

Figure 10. Bidirectional solution profiles for the discrete and continuum FPU system and the KdV model with $m = 64$.

Finally, let us investigate whether the Talbot revival phenomenon mentioned in the introduction appears in the FPU system. Somewhat surprisingly, given the noticeable effects of dispersive quantization at long rational times, numerical experiments have failed to reveal any trace of revival.

To model the delta function initial displacement, we displace the center mass by a unit†. (This is equivalent to equipartitioning the initial energy into all the Fourier modes.) Figure 11 plots the resulting solutions, in the case of $m = 128$ masses, whose initial data is the (Fourier series for) the delta function, at the indicated long rational times. These, as always, are obtained by explicitly summing over the first m modes. Keep in mind that the Fourier series of the delta function and resulting fundamental solution to the continuum model is highly oscillatory, and only converges weakly to the distributional revival profile, consisting of a finite linear combination of delta functions, at rational times. The first column plots the solutions to the bidirectional KdV model; the discrete oscillatory peaks indicate the appearance of a revival. The second column plots the corresponding FPU solution; here, there is no appreciable sign of concentration of the solution profiles and hence no apparent revival. Similar behaviors have been observed at other (long) times, with varying number of masses. The KdV profiles are fractal at irrational times and concentrated in accordance with a revival at rational times, whereas the FPU profiles are more or less uniformly oscillatory at all times.

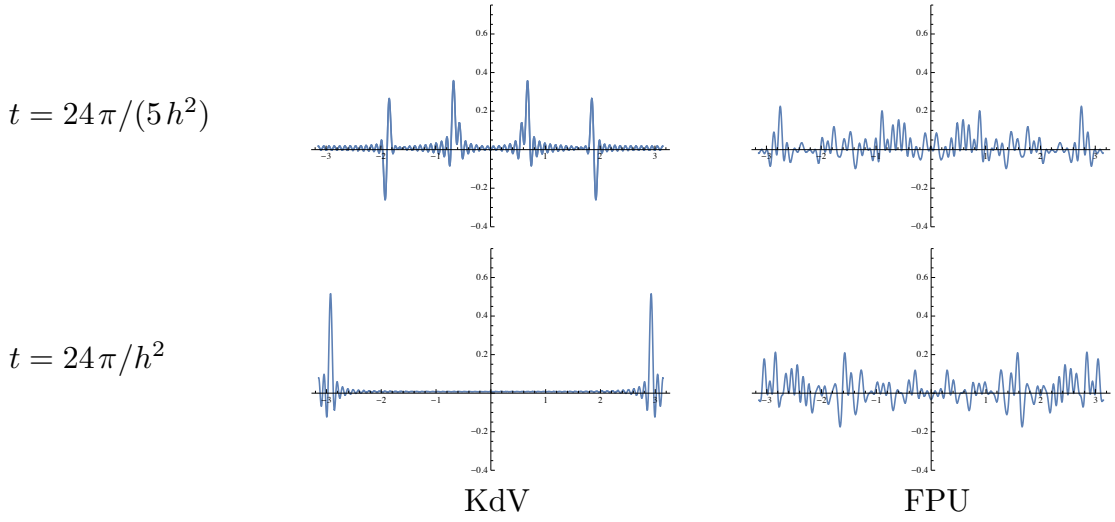

Figure 11. Revival and lack thereof.

4. Discussion.

In conclusion, we have shown that the solution to the periodic linear Fermi–Pasta–Ulam chain, with a step function as initial displacement and zero initial velocity, exhibits a fractal-like solution profile at large times, namely $t = \mathrm{O}(h^{-2}) = \mathrm{O}(m^2)$, where m is the number of masses, and h their spacing around the unit circle. Of course, being purely discrete, the solution cannot be genuinely fractal, even when extended into a continuous trigonometric interpolating function, because it only involves a sum over a finite number of Fourier modes. Moreover, it does not become fractal in the final $h \to 0$ limit since the

† Since we are dealing with a linear system, the magnitude of the displacement of the single mass does not, modulo rescaling, affect the response.

limiting equation is merely the very basic linear second order wave equation (3.16), whose solution is a combination of traveling waves, and hence piecewise constant at all times. Indeed, as $h \to 0$, all of the observed behavior on medium and long time scales moves off to infinity, and the solution converges (weakly) to the corresponding solution to the simple limiting wave equation, with all times now being classified as "short". On the other hand, all of the regularized bidirectional continuum models have genuinely fractal solutions at a dense set of times, as established in [**12**], which closely follow the FPU solution at the given resolution. In contrast, the bi- and uni-directional Korteweg–deVries models mimic the FPU and Boussinesq solutions at irrational times, but exhibit a very different dispersive quantization profile at rational times. On the other hand, the latter solutions retain an observable trace of the overall quantized character within their fractal profiles. Finally, the lack of any noticeable form of revival in the FPU system is, in light of the previous results, surprising and not well understood.

The next stage of this project will be to investigate which of these properties, if any, carry over to the nonlinear FPU systems and other nonlinear lattices of interest. Keeping in mind the numerical observations of dispersive quantization in the Korteweg–deVries equation and its generalizations, [**8**], I expect that this will indeed be the case. Numerical schemes that retain accuracy over long times, perhaps arising from geometric integration, e.g., a Stormer–Verlet scheme, [**17**], will be essential to this endeavor.

Acknowledgments: I thank Rajendra Beekie, Gong Chen, Burak Erdoğan, Natalie Sheils, Ari Stern, and Ferdinand Verhulst for helpful discussions and correspondence on FPU and fractalization.

References

[**1**] Berry, M.V., Quantum fractals in boxes, *J. Phys. A* **29** (1996), 6617–6629.

[**2**] Berry, M.V., and Klein, S., Integer, fractional and fractal Talbot effects, *J. Mod. Optics* **43** (1996), 2139–2164.

[**3**] Berry, M.V., Marzoli, I., and Schleich, W., Quantum carpets, carpets of light, *Physics World* **14**(6) (2001), 39–44.

[**4**] Bona, J.L., and Saut, J.–C., Dispersive blowup of solutions of generalized Korteweg–de Vries equations, *J. Diff. Eq.* **103** (1993), 3–57 .

[**5**] Boussinesq, J., Essai sur la théorie des eaux courantes, *Mém. Acad. Sci. Inst. Nat. France* **23** (1) (1877), 1–680.

[**6**] Bruggeman, R., and Verhulst, F., Near-integrability and recurrence in FPU chains with alternating masses, *J. Nonlinear Sci.* **29** (2019), 183–206.

[**7**] Calogero, F., Solution of the one-dimensional n-body problems with quadratic and/or inversely quadratic pair potentials, *J. Math. Phys.* **12** (1971), 419–436.

[**8**] Chen, G., and Olver, P.J., Dispersion of discontinuous periodic waves, *Proc. Roy. Soc. London A* **469** (2013), 20120407.

[**9**] Chousionis, V., Erdoğan, M.B., and Tzirakis, N., Fractal solutions of linear and nonlinear dispersive partial differential equations, *Proc. London Math. Soc.* **110** (2015), 543–564.

[**10**] Daripa, P., and Hua, W., A numerical study of an ill-posed Boussinesq equation arising in water waves and nonlinear lattices: Filtering and regularization techniques, *Appl. Math. Comput.* **101** (1999), 159–207.

[**11**] Drazin, P.G., and Johnson, R.S., *Solitons*: *An Introduction*, Cambridge University Press, Cambridge, 1989.

[**12**] Erdoğan, M.B., and Shakan, G., Fractal solutions of dispersive partial differential equations on the torus, *Selecta Math.* **25** (2019), 11.

[**13**] Erdoğan, M.B., and Tzirakis, N., Talbot effect for the cubic nonlinear Schrödinger equation on the torus, *Math. Res. Lett.* **20** (2013), 1081–1090.

[**14**] Erdoğan, M.B., and Tzirakis, N., *Dispersive Partial Differential Equations: Wellposedness and Applications*, London Math. Soc. Student Texts, vol. 86, Cambridge University Press, Cambridge, 2016.

[**15**] Fermi, E., Pasta, J., and Ulam, S., Studies of nonlinear problems. I., Los Alamos Report LA1940, 1955, *in*: *Nonlinear Wave Motion*, A.C. Newell, ed., Lectures in Applied Math., vol. 15, American Math. Soc., Providence, R.I., 1974, pp. 143–156.

[**16**] Galgani, L., Giorgilli, A., Martinoli, A., and Vanzini, S., On the problem of energy partition for large systems of the Fermi–Pasta–Ulam type: analytical and numerical estimates, *Physica D* **59** (1992), 334–348.

[**17**] Hairer, E., Lubich, C., and Wanner, G., *Geometric Numerical Integration*, Springer–Verlag, New York, 2002.

[**18**] Lennard–Jones, J.E., On the determination of molecular fields, *Phys. Rev. A* **5** (1972), 1372–1376.

[**19**] Moser, J., Three integrable Hamiltonian systems connected with isospectral deformations, *Adv. Math.* **16** (1975), 197–220.

[**20**] Olver, P.J., Dispersive quantization, *Amer. Math. Monthly* **117** (2010), 599–610.

[**21**] Olver, P.J., *Introduction to Partial Differential Equations*, Undergraduate Texts in Mathematics, Springer, New York, 2014.

[**22**] Olver, P.J., and Shakiban, C., *Applied Linear Algebra*, Second Edition, Undergraduate Texts in Mathematics, Springer, New York, 2018.

[**23**] Olver, P.J., and Tsatis, E., Points of constancy of the periodic linearized Korteweg–deVries equation, *Proc. Roy. Soc. London A* **474** (2018), 20180160.

[**24**] Oskolkov, K.I., A class of I.M. Vinogradov's series and its applications in harmonic analysis, *in*: *Progress in Approximation Theory*, Springer Ser. Comput. Math., 19, Springer, New York, 1992, pp. 353–402.

[**25**] Pankov, A., *Travelling Waves and Periodic Oscillations in Fermi–Pasta–Ulam Lattices*, Imperial College Press, London, 2005.

[**26**] Rodnianski, I., Fractal solutions of the Schrödinger equation, *Contemp. Math.* **255** (2000), 181–187.

[**27**] Rosenau, P., Dynamics of nonlinear mass-spring chains near the continuum limit, *Phys. Lett. A* **118** (1986), 222–227.

[**28**] Rosenau, P., Dynamics of dense lattices, *Phys. Rev. B* **36** (1987), 5868–5876.

[**29**] Scott, A.C., Soliton oscillations in DNA, *Phys. Rev. A* **31** (1985), 3518–3519.

[**30**] Smoller, J., *Shock Waves and Reaction–Diffusion Equations*, 2nd ed., Springer–Verlag, New York, 1994.

[**31**] Sutherland, B., Exact results for a quantum many-body problem in one-dimension. II, *Phys. Rev. A* **5** (1972), 1372–1376.

[**32**] Talbot, H.F., Facts related to optical science. No. IV, *Philos. Mag.* **9** (1836), 401–407.

[**33**] Toda, M., *Theory of Nonlinear Lattices*, Springer–Verlag, New York, 1981.

[**34**] Ulam, S.M., *Adventures of a Mathematician*, Scribner, New York, 1976.

[**35**] Vrakking, M.J.J., Villeneuve, D.M., and Stolow, A., Observation of fractional revivals of a molecular wavepacket, *Phys. Rev. A* **54** (1996), R37–40.

[**36**] Whitham, G.B., *Linear and Nonlinear Waves*, John Wiley & Sons, New York, 1974.

[**37**] Yeazell, J.A., and Stroud, C.R., Jr., Observation of fractional revivals in the evolution of a Rydberg atomic wave packet, *Phys. Rev. A* **43** (1991), 5153–5156.

[**38**] Zabusky, N.J., Computational synergetics and mathematical innovation, *J. Comp. Phys.* **43** (1981), 195–249.

[**39**] Zabusky, N.J., and Deem, G.S., Dynamics of nonlinear lattices I. Localized optical excitations, acoustic radiation, and strong nonlinear behavior, *J. Comp. Phys.* **2** (1967), 126–153.

[**40**] Zabusky, N.J., and Kruskal, M.D., Interaction of "solitons" in a collisionless plasma and the recurrence of initial states, *Phys. Rev. Lett.* **15** (1965), 240–243.